Available online at www.sciencedirect.com
ScienceDirect
Journal of Sound and Vibration 309 (2008) 695–717
JOURNAL OF SOUND AND VIBRATION
www.elsevier.com/locate/jsvi

On the tuning of variable piezoelectric transducer circuitry network for structural damage identification

L.J. Jiang[a,*], J. Tang[b], K.W. Wang[a]

[a]*Department of Mechanical & Nuclear Engineering, The Pennsylvania State University, University Park, PA 16802, USA*
[b]*Department of Mechanical Engineering, University of Connecticut, Storrs, CT 06269, USA*

Received 19 March 2006; received in revised form 11 September 2006; accepted 26 July 2007
Available online 10 September 2007

Abstract

The concept of using piezoelectric transducer circuitry with tunable inductance has been recently proposed to enhance the performance of frequency-shift-based damage identification method. While this approach has shown promising potential, a piezoelectric circuitry tuning methodology that can yield the optimal damage identification performance has not been synthesized. This research aims at advancing the state-of-the-art by exploring the characteristics of inductance tuning such that the enrichment of frequency measurements can be effectively realized to highlight the damage occurrence. Analysis shows that when the inductance is tuned to accomplish eigenvalue curve veering, the change of system eigenvalues induced by structural damage will vary significantly with respect to the change of inductance. Therefore, by tuning the inductance near the curve-veering range, one may obtain *a family of* frequency response functions that could effectively reflect the damage occurrence. When multiple tunable piezoelectric transducer circuitries are integrated to the mechanical structure, multiple eigenvalue curve veering can be simultaneously accomplished, and a series of inductance tunings can be formed by accomplishing curve veering between different pairs of system eigenvalues. It will then be shown that, to best characterize the damage occurrence, the favorable inductance tuning sequence should be selected as that leads to a "comprehensive" set of eigenvalue curve veering, i.e., all measurable natural frequencies undergo curve veering at least once. An iterative second-order perturbation-based algorithm is used to identify the locations and severities of the structural damages based on the frequency measurements before and after the damage occurrence. Numerical analyses on benchmark beam and plate structures have been carried out to examine the system performance. The effects of measurement noise on the effectiveness of the proposed damage identification method are also evaluated. It is demonstrated that the damage identification results can be significantly improved by using the variable piezoelectric transducer circuitry network with the favorable inductance-tuning scheme proposed in this research.

1. Introduction

Due to its importance for various engineering systems, research on structural health monitoring [1] has been performed extensively in recent years. Among the different damage detection approaches, the vibration-based methods [2–4] have been quite popular. The basic idea of vibration-based damage identification is that damage

*Corresponding author. Tel.: +1 814 863 1986; fax: +1 814 863 7222.
E-mail addresses: jiang@psu.edu (L.J. Jiang), jtang@engr.uconn.edu (J. Tang), kwwang@psu.edu (K.W. Wang).

0022-460X/$ - see front matter © 2007 Elsevier Ltd. All rights reserved.
doi:10.1016/j.jsv.2007.07.045

Nomenclature

$\mathbf{D}_k^{(1)}$	coefficient of the first-order perturbation term for the kth system eigenvector
$\tilde{\mathbf{K}}$	generalized stiffness matrix of the electro-mechanical integrated system before damage
$\tilde{\mathbf{K}}^d$	generalized stiffness matrix of the electro-mechanical integrated system after damage
$\mathbf{K}_s$	stiffness matrix of the mechanical structure before damage
$\mathbf{K}_s^d$	stiffness matrix of the mechanical structure after damage
$\tilde{\mathbf{K}}_j^e$	elemental stiffness matrix of the jth element positioned within the global stiffness matrix $\tilde{\mathbf{K}}$
$\mathbf{K}_c$	coupling term between the mechanical and electrical fields
$\mathbf{K}_p$	inverse capacitance matrix of the piezoelectric circuitry network
$\mathbf{L}$	inductance matrix of the piezoelectric circuitry network
$\mathbf{L}^*$	critical inductances to accomplish pairs of close eigenvalues
$\tilde{\mathbf{M}}$	generalized mass matrix of the electro-mechanical integrated system
$\mathbf{M}_s$	mass matrix of the mechanical structure only
$\mathbf{q}$	displacement vector of the mechanical structure
$\mathbf{Q}$	electrical charge flow vector in the circuit
$\mathbf{S}_k^{(1)}$	coefficient of the first-order perturbation term for the kth system eigenvalue
$\mathbf{S}_k^{(2)}$	coefficient of the second-order perturbation term for the kth system eigenvalue
α_j	stiffness parameter of the jth element (value of 1.0 denotes no damage in that element)
$\delta\alpha_j$	damage-induced stiffness parameter variation of the jth element
$\delta\boldsymbol{\alpha}$	vector of elemental stiffness parameter variation
$\delta\lambda_i$	change of the ith system eigenvalue due to the structural damage
$\delta\boldsymbol{\varphi}_i$	change of the ith system eigenvector due to the structural damage
λ_i	the ith eigenvalue of the electro-mechanical integrated system before damage
λ_i^d	the ith eigenvalue of the electro-mechanical integrated system after damage
$\boldsymbol{\varphi}_i$	the ith eigenvector of the healthy integrated electro-mechanical system
$\boldsymbol{\varphi}_i^d$	the ith eigenvector of the damaged integrated electro-mechanical system

in the structure will change the structural properties (mass, stiffness and damping) and these changes will result in changes in the dynamic characteristics of the global system response, such as natural frequencies, damping ratios and mode shapes. Typically, since the measurement of natural frequencies (eigenvalues) and frequency response functions is quite straightforward [5,6], the damage detection schemes that require only the measurement of natural frequencies (hereafter referred to as the frequency-shift-based methods [7]) are considered to be the easiest to implement, which is a significant advantage especially for complex structures.

The current practice of frequency-shift-based damage identification methods, nevertheless, has severe limitations. For example, one problem is that the natural frequencies can be relatively insensitive to damage occurrence. To address this issue, Ray and Tian [8] introduced the concept of sensitivity enhancing control (SEC) to increase modal frequency sensitivity to damage. The feedback control law is designed by placing the closed-loop modal frequencies at appropriate locations so that their sensitivities toward mass or stiffness damage can be enhanced. Later, this concept was experimentally validated on a cantilevered beam [9] and extended to multi-input systems [10]. Another serious limitation of the traditional frequency-shift-based damage identification method is that the number of natural frequencies that can be accurately measured is normally much smaller than the number of system parameters required to completely characterize the damage. To address this issue, several methods have been proposed in the literature. Cha and Gu [11] and Nalitolela et al. [12] introduced a mass/stiffness addition technique to enrich the modal information measurement. However, the direct addition of mass/stiffness to a structure might be very difficult to implement for many practical applications. To overcome this difficulty, Lew and Juang [13] proposed an active control approach by using a virtual passive controller to enrich modal frequency measurement. Specifically, different feedback

controllers are incorporated to generate additional closed-loop natural frequencies. Koh and Ray [10] also addressed this issue by utilizing multiple closed-loop systems that can lead to a much enlarged dataset of frequency measurement.

Recently, an alternative approach utilizing piezoelectric transducer circuitry with tunable inductance to enrich frequency measurement data has been proposed by Jiang et al. [14]. The key idea is to use a tunable piezoelectric circuitry coupled to the mechanical structure to favorably alter the dynamics of the electro-mechanical integrated system. First, the circuitry can be tailored to change the system frequency/modal distribution by introducing additional resonant frequencies and vibration modes. Second, through tuning the circuitry elements (i.e., the inductors), one can obtain a much enlarged dataset consisting of a *family* of frequency response functions (under different circuitry tunings) as compared to the original single frequency response of the mechanical structure without circuit. It has been shown that this method could have the potential of more completely and accurately characterizing the variation of system dynamic response due to damage. The variable inductance can be easily achieved by utilizing synthetic inductors [15–19]. The advantages of synthetic inductors, including small size, low power, high accuracy and wide range of tuning, make for the practical realization of the proposed damage identification enhancement approach. This approach is analogs to adding extra mechanical spring–mass elements to the structure [11,12]. However, electrical tailoring with variable circuitry is much easier to implement than mechanical tailoring in real systems. On the other hand, compared with the schemes based on active feedback control [10,13], while the system presented in Ref. [14] also requires attachment of additional physical element (i.e., piezoelectric transducers) to the structure, it does not require a complex sensor–actuator–controller architecture and significant external energy source.

2. Problem statement, objective, and approach overview

Although promising features of the tunable piezoelectric circuitry have been illustrated in the previous study [14], the fundamental issue on how to tune the inductance in the circuit to yield the optimal damage identification performance has not been investigated in a systematic manner. The objective of this research is to address this issue and advance the state-of-the-art of utilizing tunable piezoelectric circuitry for damage identification enhancement. Specifically, we will study the underlying mechanism of system dynamics variation under various circuitry inductance tunings. In this paper, it will be shown that eigenvalue curve veering can be accomplished by properly tuning the circuitry inductance. The occurrence of eigenvalue curve-veering produces an inductance tuning range in which high sensitivity of damaged-induced eigenvalue change with respect to inductance variation can be expected. Therefore, by tuning the inductance inside the curve-veering range, one may obtain a series of frequency response functions that could reflect the damage occurrence more thoroughly. Moreover, when multiple tunable piezoelectric transducer circuitries are integrated to the mechanical structure, multiple eigenvalue curve veering can be simultaneously accomplished, and the possibility of accomplishing curve veering between different pairs of system eigenvalues provides us with more flexibility in inductance tuning. It will then be shown that, to best characterize the damage occurrence, the favorable inductance tuning sequence should be selected as that it leads to a "comprehensive" set of eigenvalue curve veering, i.e., all measurable natural frequencies undergo curve veering at least once. Throughout this research, an iterative second-order perturbation based algorithm is used to identify the locations and severities of the structural damages based on the frequency measurements before and after the damage occurrence. Numerical analyses on benchmark beam and plate structures demonstrate that the performance of damage identification can be significantly improved by using the variable piezoelectric transducer circuitry network with the inductance tuning method proposed in this research.

3. Damage identification using tunable piezoelectric transducer circuitry network

When a network of piezoelectric transducer circuitry with tunable inductors is integrated to a structure to form an electro-mechanical integrated system, the equations of motion of the integrated system

can be written as [20–23]

$$\begin{bmatrix} \mathbf{M}_s & \mathbf{0} \\ \mathbf{0} & \mathbf{L} \end{bmatrix} \begin{Bmatrix} \ddot{\mathbf{q}} \\ \ddot{\mathbf{Q}} \end{Bmatrix} + \begin{bmatrix} \mathbf{C} & \mathbf{0} \\ \mathbf{0} & \mathbf{R} \end{bmatrix} \begin{Bmatrix} \dot{\mathbf{q}} \\ \dot{\mathbf{Q}} \end{Bmatrix} + \begin{bmatrix} \mathbf{K}_s & \mathbf{K}_c \\ \mathbf{K}_c^{\mathrm{T}} & \mathbf{K}_p \end{bmatrix} \begin{Bmatrix} \mathbf{q} \\ \mathbf{Q} \end{Bmatrix} = \begin{Bmatrix} \mathbf{F}_d \\ \mathbf{0} \end{Bmatrix}, \tag{1}$$

where $\mathbf{q}$ is the displacement vector of the structure, $\mathbf{Q}$ is the electrical charge flow vector in the circuit, $\mathbf{M}_s$, $\mathbf{C}$, and $\mathbf{K}_s$ are the mass, damping and stiffness matrices of the mechanical structure, respectively, $\mathbf{L}$, $\mathbf{R}$, and $\mathbf{K}_p$ are the inductance, resistance, and inverse capacitance matrices of the circuit, respectively, $\mathbf{K}_c$ is the coupling term between the mechanical and electrical fields, and $\mathbf{F}_d$ is the external disturbance/excitation. The generalized mass and stiffness matrices of the electro-mechanical integrated system can be written as

$$\tilde{\mathbf{M}} = \begin{bmatrix} \mathbf{M}_s & \mathbf{0} \\ \mathbf{0} & \mathbf{L} \end{bmatrix}, \quad \tilde{\mathbf{K}} = \begin{bmatrix} \mathbf{K}_s & \mathbf{K}_c \\ \mathbf{K}_c^T & \mathbf{K}_p \end{bmatrix}. \tag{2a,b}$$

Neglecting damping, we can obtain the eigenvalue problems of the integrated system associated with the undamaged (healthy) structure and damaged structure, respectively,

$$(-\lambda_i \tilde{\mathbf{M}} + \tilde{\mathbf{K}})\boldsymbol{\varphi}_i = \mathbf{0}, \tag{3}$$

$$(-\lambda_i^d \tilde{\mathbf{M}}^d + \tilde{\mathbf{K}}^d)\boldsymbol{\varphi}_i^d = \mathbf{0}, \tag{4}$$

where λ_i and $\boldsymbol{\varphi}_i$ are the ith eigenvalue and eigenvector of the undamaged system, respectively, and λ_i^d, $\boldsymbol{\varphi}_i^d$ are the ith eigenvalue and eigenvector of the damaged system, respectively. In this research, we are concerned with the structural damage that only induces the change of structural stiffness. Thus,

$$\tilde{\mathbf{M}}^d = \tilde{\mathbf{M}}, \quad \tilde{\mathbf{K}}^d = \tilde{\mathbf{K}} + \delta\tilde{\mathbf{K}}. \tag{5a,b}$$

Assuming that the damage results in eigenvalue change $\delta\lambda_i$ and eigenvector change $\delta\boldsymbol{\varphi}_i$, we then have

$$\lambda_i^d = \lambda_i + \delta\lambda_i, \quad \boldsymbol{\varphi}_i^d = \boldsymbol{\varphi}_i + \delta\boldsymbol{\varphi}_i. \tag{6a,b}$$

Substituting Eqs. (5a,b) and (6a,b) into Eq. (4) and neglecting the high-order terms, we can obtain a first-order approximation

$$\delta\lambda_i = (\boldsymbol{\varphi}_i)^{\mathrm{T}} \delta\tilde{\mathbf{K}}(\boldsymbol{\varphi}_i). \tag{7}$$

In a finite element model, the change of the global stiffness matrix can be expressed as the summation of elemental stiffness matrix changes,

$$\delta\tilde{\mathbf{K}} = \sum_{j=1}^{n_e} \delta\alpha_j \cdot \tilde{\mathbf{K}}_j^e, \tag{8}$$

where $\tilde{\mathbf{K}}_j^e$ is the elemental stiffness matrix of the jth element positioned within the generalized stiffness matrix of the integrated system $\tilde{\mathbf{K}}$, and $\delta\alpha_j = \alpha_j^d - \alpha_j^h$ denotes the damage-induced stiffness parameter variation of the jth element.

Collecting all the available changes of the respective eigenvalues, we may formulate a first-order sensitivity based equation relating the vector of damage-induced eigenvalue changes ($\delta\boldsymbol{\lambda}$) to the vector of damage-induced stiffness parameter variation ($\delta\boldsymbol{\alpha}$) as follows:

$$\delta\boldsymbol{\lambda} = \mathbf{S} \cdot \delta\boldsymbol{\alpha}, \tag{9}$$

where $\delta\boldsymbol{\lambda} = [\,\delta\lambda_1 \quad \delta\lambda_2 \quad \cdots \quad \delta\lambda_m\,]^{\mathrm{T}}$ in which m is the number of measured (available) natural frequencies of the integrated system, $\delta\boldsymbol{\alpha} = [\,\delta\alpha_1 \quad \delta\alpha_2 \quad \cdots \quad \delta\alpha_{n_e}\,]^{\mathrm{T}}$ in which n_e is the number of structural elements in the finite element model, and $\mathbf{S} \in \mathrm{Re}^{m \times n_e}$ is the first-order sensitivity matrix whose elements can be calculated by using the following equation:

$$\mathbf{S}(i,j) = (\boldsymbol{\varphi}_i)^{\mathrm{T}} \tilde{\mathbf{K}}_j^e (\boldsymbol{\varphi}_i). \tag{10}$$

Since in general, the number of measured frequencies (m) is much smaller than the number of structural elements, n_e, Eq. (9) is a significantly underdetermined problem.

One of the key features of integrating tunable piezoelectric transducer circuitry to the structure is that we will be able to obtain multiple frequency response functions (with different inductances) and their changes due to (the same) damage, which leads to a much enlarged dataset for damage detection and identification. Let the inductances in the piezoelectric transducer circuitry network be tuned to form a sequence $\mathbf{L}^{(i)}(i=1,2,\cdots,n)$

$$\begin{bmatrix} \mathbf{L}^{(1)} \\ \mathbf{L}^{(2)} \\ \vdots \\ \mathbf{L}^{(n)} \end{bmatrix} = \begin{bmatrix} L_1^{(1)} & L_2^{(1)} & \cdots & L_p^{(1)} \\ L_1^{(2)} & L_2^{(2)} & \cdots & L_p^{(2)} \\ \vdots & \vdots & \vdots & \vdots \\ L_1^{(n)} & L_2^{(n)} & \cdots & L_p^{(n)} \end{bmatrix}, \tag{11}$$

where the number of columns, p, represents the number of tunable piezoelectric transducer circuitries integrated to the mechanical structure, and the number of rows, n, represents the number of inductance tuning sets. A set of simultaneous equations similar to Eq. (9) can then be obtained and these equations can be written in the matrix form as follows:

$$\begin{bmatrix} \delta\boldsymbol{\lambda}(\mathbf{L}^{(1)}) \\ \delta\boldsymbol{\lambda}(\mathbf{L}^{(2)}) \\ \vdots \\ \delta\boldsymbol{\lambda}(\mathbf{L}^{(n)}) \end{bmatrix} = \begin{bmatrix} \mathbf{S}(\mathbf{L}^{(1)}) \\ \mathbf{S}(\mathbf{L}^{(2)}) \\ \vdots \\ \mathbf{S}(\mathbf{L}^{(n)}) \end{bmatrix} \cdot \delta\boldsymbol{\alpha}. \tag{12}$$

This formulation clearly illustrates the advantage of using tunable piezoelectric circuitry. We can now significantly increase the number of measurements in eigenvalue changes (or frequency shifts) and thus increase the number of simultaneous equations that characterize the damage features. In other words, we can make the problem much less underdetermined.

The main limitation of the above first-order approximation based algorithm is that the information regarding the change in eigenvectors (mode shapes) is not included, which could deteriorate the accuracy of damage identification. Recently, Wong et al. [24] developed a general high-order perturbation expression for eigenvalue problem with changes in stiffness, and the perturbation method is used iteratively in conjunction with an optimization method to identify the stiffness variations in the structure. In what follows, we use a second-order perturbation to describe the changes of eigenvalues, which incorporates the prediction of changes of mode shapes in the derivation. The changes of the kth eigenvalue of the integrated system after damage occurrence can be expressed as

$$\delta\lambda_k = \sum_{i=1}^{n_e} \frac{\partial\lambda_k}{\partial\alpha_i}\delta\alpha_i + \sum_{i=1}^{n_e}\sum_{j=1}^{n_e} \frac{\partial^2\lambda_k}{\partial\alpha_i\partial\alpha_j}\delta\alpha_i\delta\alpha_j = \mathbf{S}_k^{(1)}\delta\boldsymbol{\alpha} + \delta\boldsymbol{\alpha}^{\mathrm{T}}\mathbf{S}_k^{(2)}\delta\boldsymbol{\alpha}, \tag{13}$$

where $\mathbf{S}_k^{(1)}$ and $\mathbf{S}_k^{(2)}$ are the coefficients of the first and second-order perturbations for the kth eigenvalue, respectively,

$$\mathbf{S}_k^{(1)}(i) = (\boldsymbol{\varphi}_k)^{\mathrm{T}}\tilde{\mathbf{K}}_i^e(\boldsymbol{\varphi}_k), \tag{14}$$

$$\mathbf{S}_k^{(2)}(i,j) = \frac{1}{2!}(\boldsymbol{\varphi}_k)^{\mathrm{T}}\{\tilde{\mathbf{K}}_i^e\mathbf{D}_k^{(1)}(j) + \tilde{\mathbf{K}}_j^e\mathbf{D}_k^{(1)}(i)\}, \tag{15}$$

where $\mathbf{D}_k^{(1)}(i)$ is the coefficient vector of the first-order perturbation for the kth mass-normalized eigenvector

$$\delta\boldsymbol{\varphi}_k = \sum_{i=1}^{n_e} \frac{\partial\boldsymbol{\varphi}_k}{\partial\alpha_i}\delta\alpha_i = \sum_{i=1}^{n_e} \mathbf{D}_k^{(1)}(i)\delta\alpha_i \tag{16}$$

and can be calculated as follows:

$$\mathbf{D}_k^{(1)}(i) = \sum_{j=1}^{m} \mathbf{P}_k^{(1)}(i,j)\boldsymbol{\varphi}_j, \tag{17}$$

$$\mathbf{P}_k^{(1)}(i,j) = \begin{cases} 0, & j = k, \\ \frac{1}{\lambda_k - \lambda_j}(\boldsymbol{\varphi}_j)^{\mathrm{T}} \tilde{\mathbf{K}}_i^e(\boldsymbol{\varphi}_k), & j \neq k. \end{cases} \tag{18}$$

For a given set of inductance tuning, $\mathbf{L}^{(0)} = [\,L_1^{(0)} \quad L_2^{(0)} \quad \cdots \quad L_p^{(0)}\,]$, a second-order perturbation-based equation can be obtained as

$$\begin{aligned} \delta\boldsymbol{\lambda}(\mathbf{L}^{(0)}) &= \begin{Bmatrix} \delta\lambda_1(\mathbf{L}^{(0)}) \\ \delta\lambda_2(\mathbf{L}^{(0)}) \\ \vdots \\ \delta\lambda_m(\mathbf{L}^{(0)}) \end{Bmatrix} = \begin{bmatrix} \mathbf{S}_1^{(1)} \\ \mathbf{S}_2^{(1)} \\ \vdots \\ \mathbf{S}_m^{(1)} \end{bmatrix} \cdot \delta\boldsymbol{\alpha} + \begin{bmatrix} (\delta\boldsymbol{\alpha})^{\mathrm{T}}\mathbf{S}_1^{(2)}(\delta\boldsymbol{\alpha}) \\ (\delta\boldsymbol{\alpha})^{\mathrm{T}}\mathbf{S}_2^{(2)}(\delta\boldsymbol{\alpha}) \\ \vdots \\ (\delta\boldsymbol{\alpha})^{\mathrm{T}}\mathbf{S}_m^{(2)}(\delta\boldsymbol{\alpha}) \end{bmatrix} \\ &= \mathbf{S}^{(1)}(\mathbf{L}^{(0)}) \cdot \delta\boldsymbol{\alpha} + \mathbf{P}\{\mathbf{S}^{(2)}(\mathbf{L}^{(0)}), \delta\boldsymbol{\alpha}\}. \end{aligned} \tag{19}$$

When we tune the inductances to form a sequence as $\mathbf{L}^{(i)}(i = 1, 2, \cdots, n)$ and perform frequency (eigenvalue) measurements, correspondingly we may obtain a series of eigenvalue change equations, which, collectively, lead to a set of equations in the following form:

$$\begin{bmatrix} \delta\boldsymbol{\lambda}(\mathbf{L}^{(1)}) \\ \delta\boldsymbol{\lambda}(\mathbf{L}^{(2)}) \\ \vdots \\ \delta\boldsymbol{\lambda}(\mathbf{L}^{(n)}) \end{bmatrix} = \begin{bmatrix} \mathbf{S}^{(1)}(\mathbf{L}^{(1)}) \\ \mathbf{S}^{(1)}(\mathbf{L}^{(2)}) \\ \vdots \\ \mathbf{S}^{(1)}(\mathbf{L}^{(n)}) \end{bmatrix} \cdot \delta\boldsymbol{\alpha} + \begin{bmatrix} \mathbf{P}\{\mathbf{S}^{(2)}(\mathbf{L}^{(1)}), \delta\boldsymbol{\alpha}\} \\ \mathbf{P}\{\mathbf{S}^{(2)}(\mathbf{L}^{(2)}), \delta\boldsymbol{\alpha}\} \\ \vdots \\ \mathbf{P}\{\mathbf{S}^{(2)}(\mathbf{L}^{(n)}), \delta\boldsymbol{\alpha}\} \end{bmatrix}. \tag{20}$$

For the nonlinear Eq. (20), a constrained optimization can be formulated to find the approximate solution of $\delta\boldsymbol{\alpha}$. The objective of the constrained optimization is to minimize the norm of the difference between the actual eigenvalue change ($\delta\boldsymbol{\lambda}^{\text{actual}}$) from the frequency response measurement, and $\delta\boldsymbol{\lambda}(\delta\boldsymbol{\alpha})$, the eigenvalue change due to the estimated stiffness parameter variation $\delta\boldsymbol{\alpha}$, in the following manner:

$$\text{Minimize} \quad \left\|\delta\boldsymbol{\lambda}(\delta\boldsymbol{\alpha}) - \delta\boldsymbol{\lambda}^{\text{actual}}\right\|, \tag{21}$$

$$\text{subject to}: -1 < \delta\alpha_j \leq 0, \text{ where } j = 1, 2, \ldots, n_e.$$

The perturbation method is used iteratively in conjunction with the constrained optimization scheme, which yields an iterative second-order sensitivity-based damage identification algorithm.

4. Formulation of favorable inductance tuning

A fundamental issue of the proposed tunable piezoelectric circuitry concept is how to tune the inductances to optimize the improvement of the performance of damage identification. In this section, we present the guidelines of forming a favorable inductance tuning sequence based on the analysis on how the inductance tuning affects the characteristics of system dynamics and the damage-induced eigenvalue changes. First, a benchmark beam structure integrated with a single tunable piezoelectric transducer circuitry is used to obtain the fundamental understandings of the effects of inductance tuning. Then, a more complicated plate structure integrated with multiple piezoelectric transducer circuitries is studied to verify and extend the observations to multiple inductance tunings.

4.1. Integrated system with single tunable piezoelectric circuitry

We first study a benchmark example of cantilevered beam integrated with a single tunable piezoelectric transducer circuitry (Fig. 1). A circuit with tunable inductor is integrated to a homogenous cantilevered beam through the piezoelectric transducer, which is bonded on the upper surface of the beam from x_1 to x_2. Using Galerkin's method to discretize the partial differential equations, we can obtain a set of ordinary differential equations in the form of Eq. (1) [21].

4.1.1. Simplified 2-dof system analysis

If only the first mode is used in the Galerkin's method, the integrated system can be modeled as a 2-dof system and the eigenvalue problem of this simplified system is given as

$$\left(\begin{bmatrix} k_{11} & k_c \\ k_c & k_p \end{bmatrix} - \lambda_i \begin{bmatrix} m_{11} & 0 \\ 0 & L \end{bmatrix} \right) \{\boldsymbol{\varphi}_i\} = \begin{Bmatrix} 0 \\ 0 \end{Bmatrix}, \tag{22}$$

which yields two eigenvalues,

$$\lambda_{1,2} = \frac{(k_{11}L + k_p m_{11}) \pm \sqrt{(k_{11}L - k_p m_{11})^2 + 4m_{11}Lk_c^2}}{2m_{11}L}. \tag{23}$$

The difference between these two eigenvalues is

$$\lambda_1 - \lambda_2 = \frac{\sqrt{(k_{11}L - k_p m_{11})^2 + 4m_{11}Lk_c^2}}{m_{11}L}. \tag{24}$$

From Eq. (24) we can derive and conclude that the difference of the two eigenvalues reaches its minimum or, in other words, the two eigenvalues are the closest, when the inductance takes the value of

$$L^* = \frac{k_p m_{11}}{k_{11}} \left(\frac{1}{1 - 2k_c^2/(k_{11}k_p)} \right). \tag{25}$$

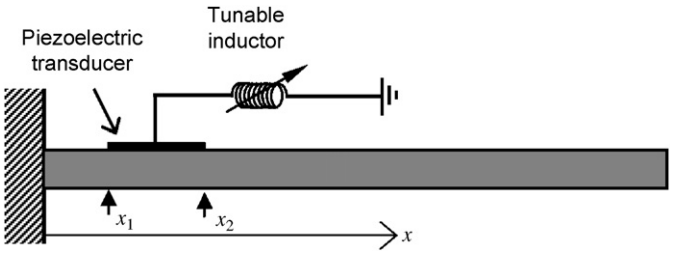

Fig. 1. Configuration of a cantilevered beam integrated with a single tunable piezoelectric transducer circuitry.

Table 1
System parameters for the integrated system of beam structure

Cantilever beam		Piezoelectric material	
Density	$\rho_b = 2700\,\mathrm{kg/m^3}$	Density	$\rho_p = 7800\,\mathrm{kg/m^3}$
Length	$L_b = 0.4184\,\mathrm{m}$	Young's modulus	$E_p = 6.6 \times 10^{10}\,\mathrm{N/m^2}$
Thickness	$h_b = 3.175\,\mathrm{mm}$	Thickness	$h_p = 0.191\,\mathrm{mm}$
Width	$b = 0.0381\,\mathrm{m}$	Dielectric constant	$\beta_{33} = 7.1445 \times 10^7\,\mathrm{V\,m/C}$
Young's modulus	$E_b = 7.1 \times 10^{10}\,\mathrm{N/m^2}$	Piezoelectric constant	$h_{31} = 1.0707 \times 10^9\,\mathrm{N/C}$

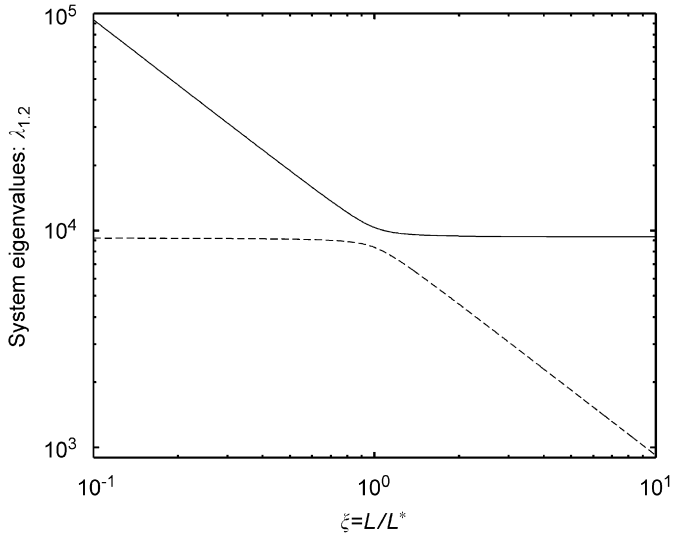

Fig. 2. System eigenvalues versus the normalized inductance when using the simplified 2-dof system model for the integrated beam system. —— λ_1, – – – – λ_2.

This is referred to as the "critical" inductance value in this paper. If we assume that $k_c^2 \leq k_{11}k_p$, Eq. (25) can be simplified as

$$L^* \approx \frac{k_p m_{11}}{k_{11}}. \tag{26}$$

Let the left and right ends of the piezoelectric transducer be $x_1 = 0.04184\,\text{m}$ and $x_2 = 0.08368\,\text{m}$. All other system parameters of this illustrative case are specified in Table 1. The variation of the two system eigenvalues with respect to the inductance tuning is plotted in Fig. 2. In this figure, the horizontal axis denotes the normalized inductance ξ, which is defined as the ratio between the actual inductance to the critical inductance L^* given in Eq. (26),

$$\xi = \frac{L}{L^*} = \frac{L}{(k_p \cdot m_{11})/k_{11}}. \tag{27}$$

From Fig. 2, we can see that the loci of the two eigenvalues approach each other in the first stage, and then diverge abruptly when we continuously increase the inductance. This phenomenon of rapid changes of system eigenvalues with respect to the system parameter (inductance L) indicates the occurrence of eigenvalue curve veering [25–28].

Liu [29] examined the derivatives of the eigenvalues and eigenvectors for the phenomena of eigenvalue curve veering and mode localization. In this paper, we are concerned with the sensitivity of damage-induced eigenvalue change with respect to inductance tuning, since a favorable tuning of the inductance value should yield a system in which the eigenvalue change is very sensitive to the damage occurrence (causing stiffness parameter change). This sensitivity can be expressed as the second-order derivatives of the system eigenvalues with respect to stiffness parameter ($G = E_b I_b$) and inductance (L),

$$\frac{\partial(\delta\lambda_{1,2})}{\partial L} = \frac{\partial}{\partial L}\left(\frac{\partial\lambda_{1,2}}{\partial G}\delta G\right) = \frac{\partial^2\lambda_{1,2}}{\partial L \partial G}\delta G. \tag{28}$$

The derivatives of the eigenvalues with respect to stiffness parameter change can be solved as

$$\frac{\partial\lambda_{1,2}}{\partial G} = \frac{\partial\lambda_{1,2}}{\partial k_{11}}\frac{\partial k_{11}}{\partial G} = \frac{1}{2m_{11}}\left[1 \pm \frac{k_{11}L - k_p m_{11}}{\sqrt{(k_{11}L - k_p m_{11})^2 + 4m_{11}Lk_c^2}}\right]\frac{\partial k_{11}}{\partial G}. \tag{29}$$

Substituting Eq. (29) into Eq. (28), we can obtain the derivative of damage-induced eigenvalue changes ($\delta\lambda_1$ and $\delta\lambda_2$) with respect to inductance (L) as

$$\frac{\partial(\delta\lambda_{1,2})}{\partial L} = \pm \frac{Lk_{11}k_c^2 + m_{11}k_pk_c^2}{\left[(k_{11}L - k_pm_{11})^2 + 4m_{11}Lk_c^2\right]^{3/2}} \left(\frac{\partial k_{11}}{\partial G}\delta G\right). \tag{30}$$

For a specific damage scenario, $(\partial k_{11}/\partial G)\delta G$ on the right-hand side of Eq. (30) is fixed, and the inductance value which yields the maximum of $\partial(\delta\lambda_{1,2})/\partial L$ can be easily solved by letting the derivative of the fraction part on the right-hand side of Eq. (30) with respect to the inductance (L) be zero,

$$L^* = \frac{m_{11}k_p}{2k_{11}} \left[\left(9 - \frac{10k_c^2}{k_{11}k_p} + \frac{k_c^4}{k_{11}^2k_p^2}\right)^{1/2} - \left(1 - \frac{k_c^2}{k_{11}k_p}\right) \right]. \tag{31}$$

If we assume that $k_c^2 \leqslant k_{11}k_p$, Eq. (31) can be simplified as

$$L^* \approx \frac{k_pm_{11}}{k_{11}}. \tag{32}$$

Assuming that the damage-induced stiffness reduction is $\delta G = -0.15G$, we can plot the derivative of the damage-induced eigenvalue changes ($\delta\lambda_1$ and $\delta\lambda_2$) with respect to inductance (L), as shown in Fig. 3. From this figure, we can see that the sensitivities of the two eigenvalue changes with respect to inductance reach their maximal absolute values when the inductance is tuned near the critical value, $L^* = k_p \cdot m_{11}/k_{11}$, and the sensitivities decreases dramatically when the inductance is tuned away from this critical value. Recall Eq. (26) and note that eigenvalue curve veering occurs when the inductance is tuned around $L^* = k_p \cdot m_{11}/k_{11}$ (Fig. 2). We can conclude that the occurrence of eigenvalue curve veering not only suggests rapid changes of system eigenvalues (characteristics of system dynamics) with respect to inductance tuning, but also produces an inductance tuning range in which high sensitivity of damaged-induced eigenvalue changes with respect to inductance tuning can be expected. Therefore, when the inductance is tuned near L^*, multiple sets of frequency-shift measurements with different sensitivity relations to the potential damage can be obtained. This can greatly enrich the frequency data available for damage identification and help to more completely capture the information about the damage occurrence.

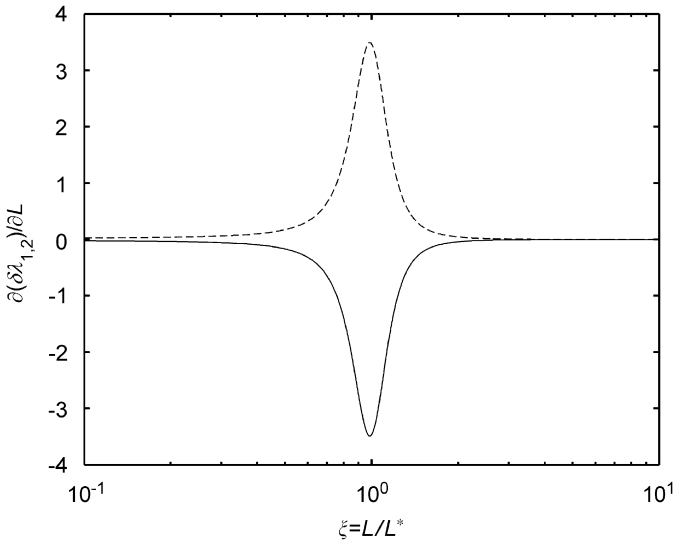

Fig. 3. Sensitivities of the damage-induced eigenvalue changes with respect to the normalized inductance when using the simplified 2-dof system model for the integrated beam system. —— $\partial(\delta\lambda_1)/\partial L$, – – – – $\partial(\delta\lambda_2)/\partial L$.

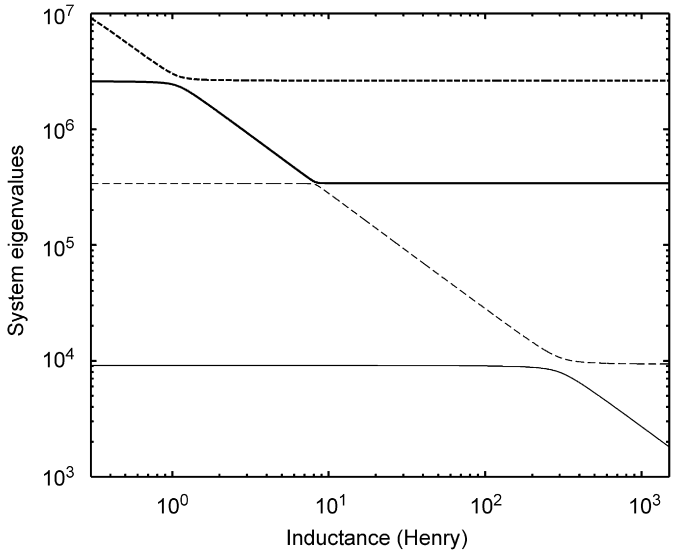

Fig. 4. System eigenvalues versus inductance when using the multiple-dof system model for the integrated beam system. —— λ_1, – – – – λ_2, ——— λ_3, - - - - λ_4.

4.1.2. Multiple-dof system analysis

The above observations for the 2-dof systems are based on the analytical sensitivity analysis of the damage-induced eigenvalue changes with respect to inductance tuning. In this sub-section we extend this sensitivity analysis to multi-dof systems. The beam shown in Fig. 1 is now analyzed using finite element analysis, where the beam is evenly discretized into 10 elements. The piezoelectric transducer is bonded on the upper surface of the beam from the second element to the fourth element. The relevant system parameters are specified in Table 1.

First, we examine how the inductance tuning alters the characteristics of system dynamics (i.e., system eigenvalues). Fig. 4 shows the variations of the first four system eigenvalues with respect to inductance tuning. From this figure, we can see that eigenvalue curve veering occurs between each two consecutive system eigenvalues from low mode to high mode when the inductance is tuned from 1500 H down to 0.3 H. In each eigenvalue curve veering, only the two associated system eigenvalues change dramatically with respect to inductance tuning, while other system eigenvalues are hardly affected. Meanwhile, as a well-known phenomenon associated with the curve veering, during the eigenvalue curve veering the eigenvectors corresponding to the veering eigenvalues will interchange in a rapid but continuous way [25,26].

It has been shown that for the 2-dof system (Figs. 2 and 3) the occurrence of eigenvalue curve veering is realized by an inductance tuning range with high sensitivity of damage-induced eigenvalue changes. In order to examine the case of a multiple-dof system, we calculate the sensitivities of the damage-induced eigenvalue changes with respect to inductance L, as plotted in Fig. 5 where (a)–(c) correspond to the first, second and third eigenvalue changes, respectively. The structural damage is assumed to be on the second beam element and the damage causes a 25% stiffness reduction. As shown in Fig. 5(a), there is only one peak region indicating high sensitivity of the first eigenvalue change with respect to inductance tuning, and this region corresponds to eigenvalue curve veering between the first and second system eigenvalues. In Fig. 5(b), two peak regions with high sensitivity of eigenvalue change with respect to inductance tuning are found, and it is easy to verify that these two regions correspond to the eigenvalue curve veering between two pairs of system eigenvalues (the first and second, and the second and third), respectively. Similar conclusion can be drawn in Fig. 5(c), where two peak regions with high sensitivity are achieved when the third system eigenvalue has curve veering with the second and fourth system eigenvalues.

Fig. 6 shows the variation of the damage-induced eigenvalue changes with respect to inductance tuning when the second element is damaged with a 25% stiffness reduction. If the inductance is tuned around each of the eigenvalue curve-veering value, the damage-induced changes of the two system eigenvalues associated with

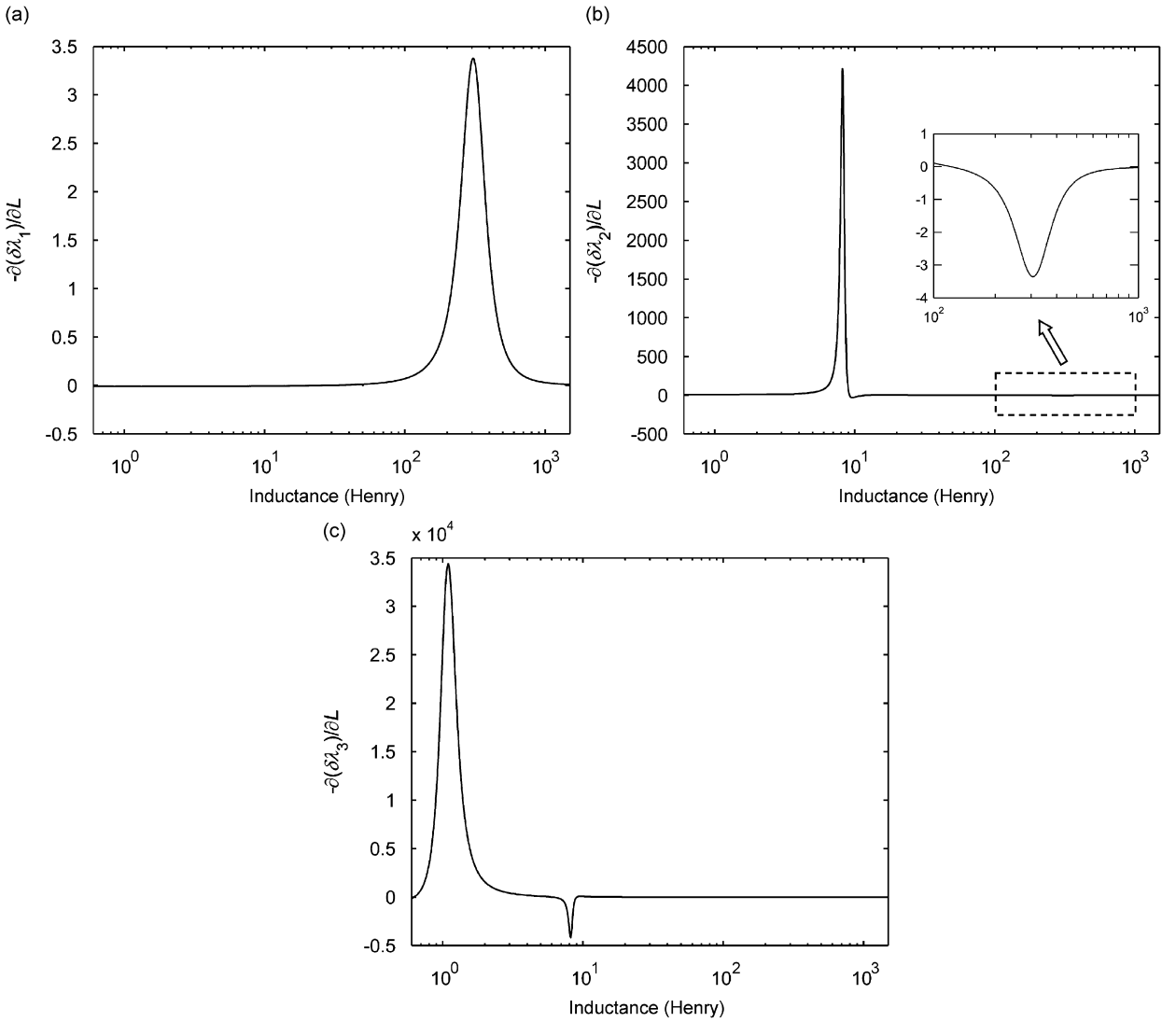

Fig. 5. Sensitivities of the damage-induced eigenvalue changes with respect to inductance when using the multiple-dof system model for the integrated beam system: (a) sensitivity of the first eigenvalue change; (b) sensitivity of the second eigenvalue change; (c) sensitivity of the third eigenvalue change.

the two loci in that curve veering vary significantly with respect to inductance. Therefore, if the inductance is tuned around values corresponding to eigenvalue curve veering, multiple sets of frequency-shift measurement with dramatically different sensitivity relations to the damage can be obtained. Again this will greatly enrich the modal data measurement available for damage identification.

4.2. Integrated system with multiple tunable piezoelectric circuitries

The previous example concerns the integration of a single tunable piezoelectric circuitry onto a homogeneous beam structure. For more complicated structures, it can be envisioned that multiple tunable circuitries could be more beneficial for damage identification. In this sub-section, we use a plate structure, as shown in Fig. 7, to explore the tuning of multiple tunable piezoelectric transducer circuitries. For this benchmark plate, the left edge of the plate is clamped and the other three edges have free boundary conditions. The plate is discretized into 25 elements, and the element numbers are labeled

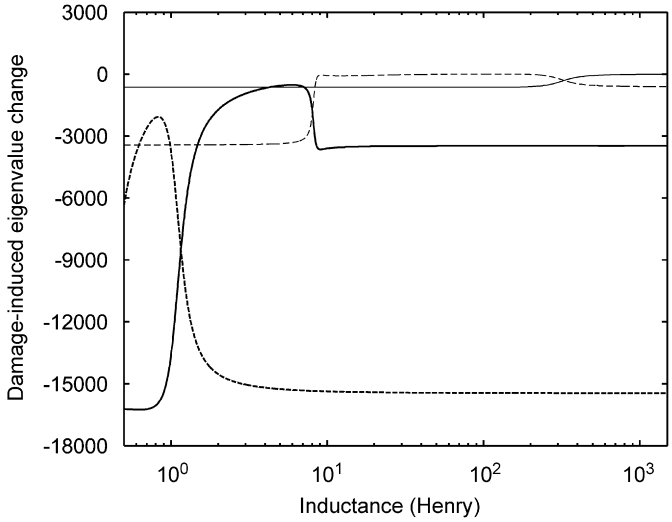

Fig. 6. Variation of the damage-induced eigenvalue changes with respect to inductance when using the multiple-dof system model for the integrated beam system. —— $\delta\lambda_1$, – – – – $\delta\lambda_2$, ▬▬▬ $\delta\lambda_3$, ▬ ▬ ▬ $\delta\lambda_4$.

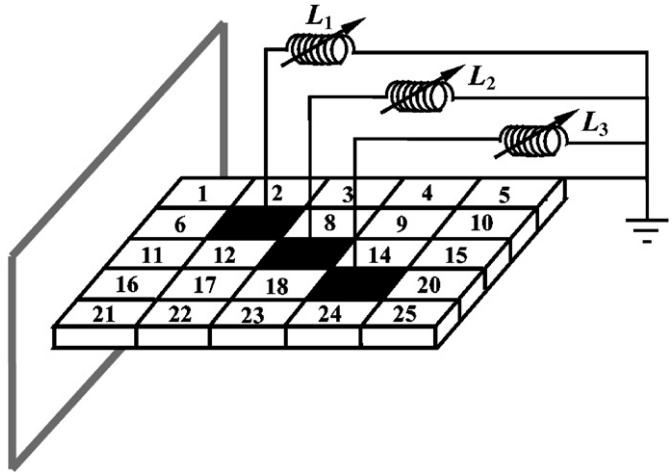

Fig. 7. Configuration of a cantilevered plate integrated with multiple tunable piezoelectric transducer circuitries.

Table 2
System parameters for the integrated system of plate structure

Plate structure		Piezoelectric material	
Density	$\rho_s = 2700\,\mathrm{kg/m^3}$	Density	$\rho_p = 7800\,\mathrm{kg/m^3}$
Length	$a = 0.25\,\mathrm{m}$	Young's modulus	$E_p = 6.9 \times 10^{10}\,\mathrm{N/m^2}$
Width	$b = 0.25\,\mathrm{m}$	Thickness	$h_p = 0.25\,\mathrm{mm}$
Thickness	$h_s = 5\,\mathrm{mm}$	Dielectric constant	$\beta_{33} = 7.1445 \times 10^7\,\mathrm{V\,m/C}$
Young's modulus	$E_s = 30 \times 10^9\,\mathrm{N/m^2}$	Piezoelectric constant	$h_{31} = 7.664 \times 10^8\,\mathrm{N/C}$
Element size	$5\,\mathrm{cm} \times 5\mathrm{cm}$	Patch size	$5\mathrm{cm} \times 5\mathrm{cm}$

as shown in the figure. Three piezoelectric transducers are bonded onto the 7th, 13th and 19th elements, respectively. Each piezoelectric transducer patch has a size of $5\,\mathrm{cm} \times 5\,\mathrm{cm}$. Three piezoelectric circuitries with tunable inductances (L_1, L_2 and L_3) are integrated to the plate structure through three piezoelectric

transducers, respectively. The parameters of the system including the plate structure and piezoelectric material are listed in Table 2.

In the case of single piezoelectric circuitry, only one eigenvalue curve veering can be achieved under certain inductance tuning, and all other eigenvalues are much less affected. On the other hand, multiple piezoelectric transducer circuitries make it possible for multiple pairs of system eigenvalues to achieve curve veering simultaneously. Such multiple curve-veering phenomena could further enhance the system response sensitivity with respect to inductance tunings. When multiple piezoelectric circuitries are integrated with the mechanical structure, these circuitries are not only directly coupled with the mechanical structure, but also coupled indirectly with other circuitries through energy exchange within the entire electro-mechanical integrated system. In other words, when tuning the inductance in one electric circuit, the interactions between the mechanical structure and other electric circuitries are also affected even if the inductances in those circuitries remain the same. Therefore, it is not feasible to tune each of the inductances separately. We need to tune these inductances simultaneously to achieve the desired set of eigenvalue curve veering concurrently. Since there are three tunable piezoelectric transducer circuitries in this plate example, these circuitries can be tuned to accomplish at least three eigenvalue curve veering. In each curve veering, one additional resonance frequency, due to the dynamics of one piezoelectric circuitry, is introduced into the frequency response function near the structural resonance frequency corresponding to that veering.

Typically, clustered eigenvalues or close natural frequencies in a dynamic system are related to eigenvalue curve veering [25–29]. Indeed, the occurrence of close eigenvalues is an indication of eigenvalue curve veering and thus can be used as the criterion for tuning the inductances to realize multiple eigenvalue curve-veering phenomena. In this research, an optimization scheme is formulated to find the critical values of three inductances $\langle L_1^*, L_2^*, L_3^* \rangle$ which yield three pairs of close eigenvalues. That is, three eigenvalue curve veerings are realized simultaneously when the inductances are tuned around their respective critical values. The objective function to be minimized is defined as the summation of the difference between each pair of system eigenvalues that are targeted for eigenvalue curve veering.

4.2.1. Option 1 of inductance tuning

The integrated system has a large number of eigenvalues/natural frequencies, which can all be potential candidates for eigenvalue curve veering. We first formulate an optimization problem to find the critical values of three inductances to achieve eigenvalue curve veering between the 1st and 2nd eigenvalues, the 3rd and 4th eigenvalues, and the 5th and 6th eigenvalues, respectively, and simultaneously. The objective function is defined as

$$J_1 = \sum_{i=1}^{3} |\lambda_{2i-1} - \lambda_{2i}|. \tag{33}$$

By using the standard constrained minimum subroutine, FMINCON, provided by MATLAB, the minimization of the above objective function yields the following critical inductance values:

$$L_1^* = 84.6\ \text{H},\ \ L_2^* = 1.91\ \text{H},\ \ L_3^* = 14.5\ \text{H}. \tag{34}$$

Utilizing the above critical values as center values and expanding the inductance on both sides by 20.0 H, 0.5 H and 4.0 H, respectively, the tuning ranges for the three inductances can be formulated as

$$L_1 \in [64.6\ \text{H},\ \ 104.6\ \text{H}],\ \ L_2 \in [1.41\ \text{H},\ \ 2.41\ \text{H}],\ \ L_3 \in [10.5\ \text{H},\ \ 18.5\ \text{H}]. \tag{35}$$

Fig. 8 shows the variation of the first six eigenvalues with respect to inductance tuning. The horizontal axis only shows the change of the inductance L_3, while it should be noted that inductances L_1 and L_2 are actually tuned synchronously when tuning L_3. (This statement holds for all the following figures in the same category.) It is shown in this figure that three eigenvalue curve veerings occur between the 1st and 2nd eigenvalues, the 3rd and 4th eigenvalues, and the 5th and 6th eigenvalues, respectively and simultaneously. Fig. 9 shows the variation of the damage-induced eigenvalue changes with respect to inductance tuning inside the proposed inductance tuning ranges. The

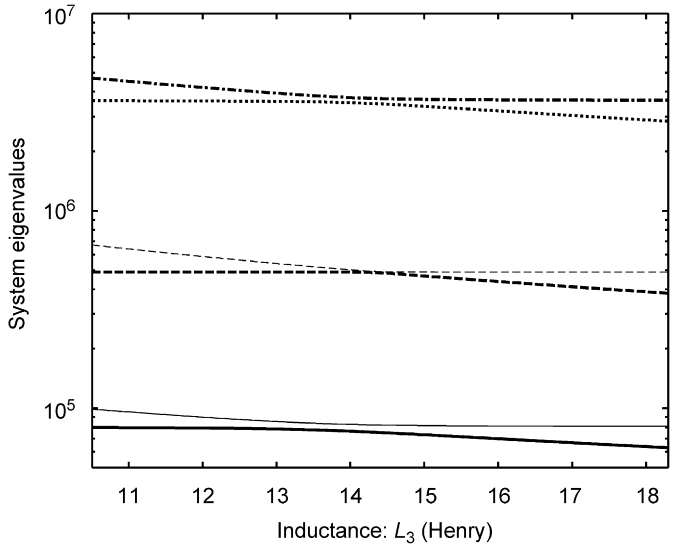

Fig. 8. System eigenvalues versus inductance L_3 for the integrated plate system when using option 1 of inductance tuning. ——— λ_1, —— λ_2, – – – λ_3, – – – – λ_4, ····· λ_5, –·–·– λ_6.

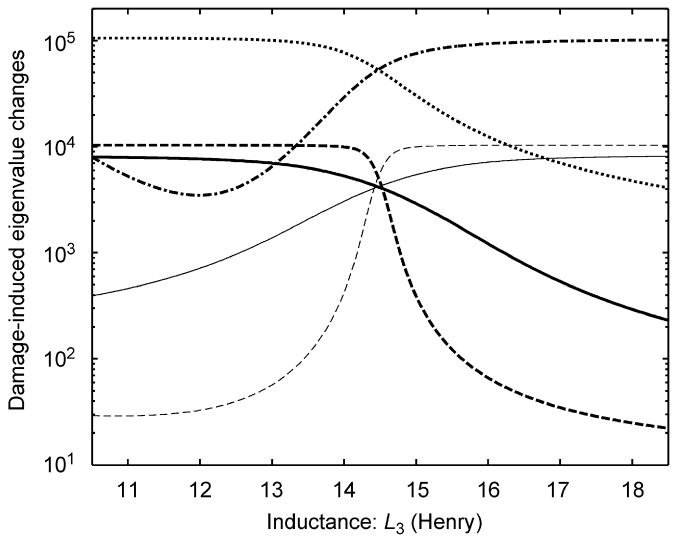

Fig. 9. Variation of the damage-induced eigenvalue changes with respect to inductance L_3 for the integrated plate system when using option 1 of inductance tuning. ——— $(-\delta\lambda_1)$, —— $(-\delta\lambda_2)$, – – – $(-\delta\lambda_3)$, – – – – $(-\delta\lambda_4)$, ····· $(-\delta\lambda_5)$, –·–·– $(-\delta\lambda_6)$.

structural damages are assumed to result in 20%, 30%, 10%, and 20% of stiffness parameter reductions on the 6th, 11th, 12th, and 16th elements, respectively. It can be easily observed from the figure that the damage-induced changes of the three eigenvalue pairs vary significantly around the curve veering values of the inductances.

4.2.2. Option 2 of inductance tuning

In order to examine the general effect of eigenvalue curve veering, here we investigate an alternative option of inductance tuning, i.e., we aim at achieving eigenvalue curve veering between the 3rd and 4th eigenvalues,

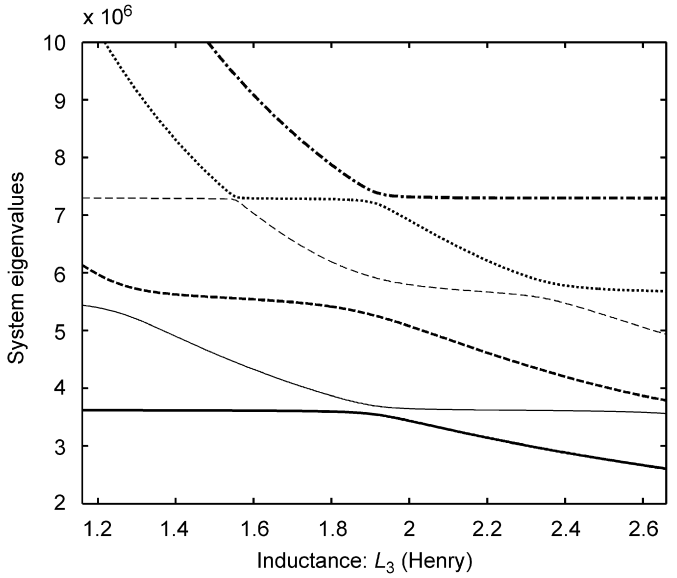

Fig. 10. System eigenvalues versus inductance L_3 for the integrated plate system when using option 2 of inductance tuning. ——— λ_3, —— λ_4, ▬ ▬ ▬ λ_5, – – – – λ_6, ▪ ▪ ▪ ▪ λ_7, ▬ · ▬ · ▬ λ_8.

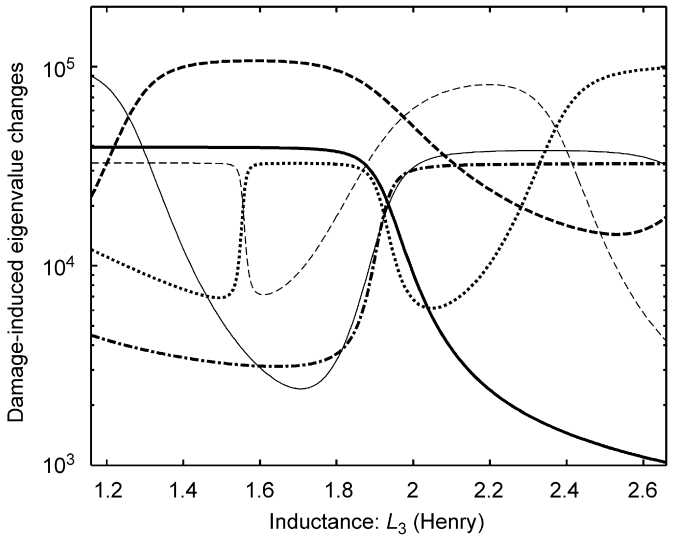

Fig. 11. Variation of the damage-induced eigenvalue changes with respect to inductance L_3 for the integrated plate system when using option 2 of inductance tuning. ——— $(-\delta\lambda_3)$, —— $(-\delta\lambda_4)$, ▬ ▬ ▬ $(-\delta\lambda_5)$, – – – – $(-\delta\lambda_6)$, ▪ ▪ ▪ ▪ $(-\delta\lambda_7)$, ▬ · ▬ · ▬ $(-\delta\lambda_8)$.

the 5th and 6th eigenvalues, and the 7th and 8th eigenvalues, respectively and simultaneously. The objective function is then defined as

$$J_2 = \sum_{i=1}^{3} \left| \lambda_{2i+1} - \lambda_{2i+2} \right|. \tag{36}$$

The minimization of the above objective function yields

$$L_1^* = 0.96 \text{ H}, \quad L_2^* = 1.25 \text{ H}, \quad L_3^* = 1.91 \text{ H}. \tag{37}$$

The tuning ranges for three inductances can be determined as

$$L_1 \in [0.51\ \text{H},\ \ 1.41\ \text{H}],\ \ L_2 \in [0.65\ \text{H},\ \ 1.85\ \text{H}],\ \ L_3 \in [1.16\ \text{H},\ \ 2.66\ \text{H}]. \tag{38}$$

The variation of the 3rd, 4th, 5th, 6th, 7th and 8th system eigenvalues with respect to inductance tuning inside the proposed tuning ranges are shown in Fig. 10. It can be observed from this figure that the eigenvalue curve veering are achieved not only between those desired pairs of system eigenvalues (the 3rd and 4th, the 5th and 6th, and the 7th and 8th), but also between the 4th and 5th, and the 6th and 7th system eigenvalues. The reason for this phenomenon is that the three circuitry modes are tuned to accomplish curve veerings with three twisting-bending modes (3rd–5th) of the plate structure, and the resonance frequencies of these twisting-bending modes are close to each other, which makes the veering more sensitive to inductance tuning. As a result, it now becomes possible for one eigenvalue to veer with its two adjacent eigenvalues successively inside the inductance tuning ranges.

For the same damage scenario as used in Fig. 9, the variations of the damage-induced eigenvalue changes with respect to inductance tuning inside the tuning ranges are plotted in Fig. 11. It can be easily seen that the variation of the damage-induced eigenvalue changes is more noticeable than that in Fig. 9 (produced under tuning option 1), and the reason for this is that additional eigenvalue veerings occur under tuning option 2, as shown in Fig. 10. Overall, we can conclude that by integrating multiple tunable piezoelectric transducer circuitries to the mechanical structure being inspected, the frequency measurement data available for damage identification can be further enriched by formulating inductance tuning sequence to accomplish eigenvalue curve veering between different pairs of system eigenvalues.

5. Damage identification analyses and case studies

The preceding sections have outlined the basis of eigenvalue curve veering under inductance tuning and illustrated such phenomena. In this section, we perform analyses on damage identification in beam and plate structures to demonstrate the performance improvement with the proposed new methodology. Specifically, we will directly utilize the favorable inductance tuning results obtained in Section 4.

5.1. Damage identification in cantilevered beam with single tunable piezoelectric circuitry

In order to illustrate the performance improvement of using tunable piezoelectric transducer circuitry network and verify the guidelines on favorable inductance tuning obtained in Section 4, here we compare the damage identification results under three different approaches: (1) the traditional method (iterative second-order perturbation-based algorithm without integration of tunable piezoelectric circuitry); (2) the enhanced integrated-system approach (iterative second-order perturbation-based algorithm with integration of tunable piezoelectric circuitry) with *ad hoc* inductance tuning; and (3) the enhanced integrated-system approach with the proposed *favorable* inductance tuning method. For a fair comparison, we assume that only the frequencies below 1000 rad/s are available for accurate measurement. This means that only the first two natural frequencies can be measured for damage identification when we use the traditional method without tunable piezoelectric circuitry, and only the first three natural frequencies, of which the additional one comes from the dynamics of the piezoelectric circuitry, are available when using the enhanced integrated-system approach. According to the analysis and results obtained in Section 4.1, a favorable inductance tuning sequence can be selected as follows:

$$\mathbf{L} = \begin{bmatrix} 7.50 & 7.75 & 8.00 & 8.25 & 8.50 & 225 & 250 & 275 & 300 & 325 \end{bmatrix} \text{H}. \tag{39}$$

In the above tuning sequence, the first 5 values are selected from the curve veering between the 2nd and 3rd system eigenvalues, and the last 5 values are selected from the curve veering between the 1st and 2nd system eigenvalues. It is worth mentioning that the large inductance values may be realized by the well-developed synthetic inductor concepts [15–19]. These electronic devices can provide a wide range of inductance tuning up to thousands of Henries, with high accuracy and high robustness against system and environmental variations.

The first case we examine is to identify single element damage. The damage in the beam is assumed to be on the 2nd element and results in a 25% stiffness reduction. Fig. 12 shows the predictions of structural damage

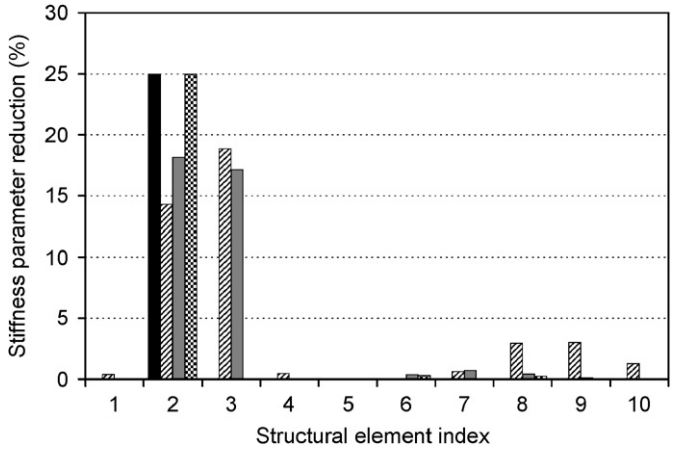

Fig. 12. Identification of structural damage on the second element of the beam structure. ■ Actual stiffness parameter reduction, ▨ prediction using the traditional method, ▩ prediction using the enhanced integrated-system approach with *ad hoc* inductance tuning, ▩ prediction using the enhanced integrated-system approach with *favorable* inductance tuning.

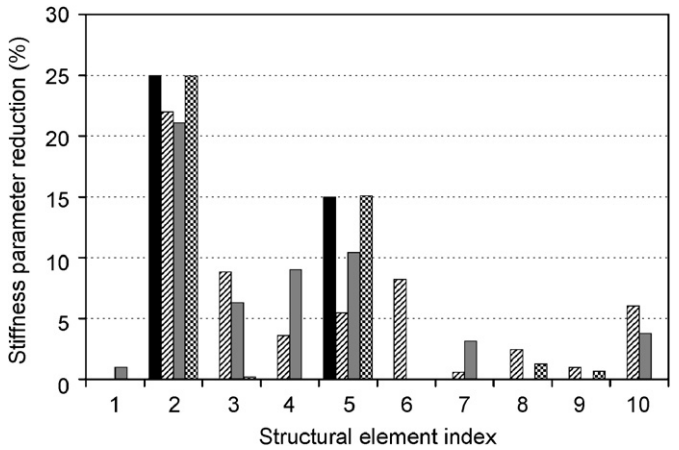

Fig. 13. Identification of structural damages on the second and fifth elements of the beam structure. ■ Actual stiffness parameter reduction, ▨ prediction using the traditional method, ▩ prediction using the enhanced integrated-system approach with *ad hoc* inductance tuning, ▩ prediction using enhanced integrated-system approach with *favorable* inductance tuning.

by using the traditional method and the enhanced integrated-system approach with *ad hoc* and *favorable* inductance tuning. From this figure, we can see that the prediction using the traditional method has significant error because the major damage is predicted to be on the 3rd element and the predicted damage severity of the 2nd element is much less than the actual value. When the enhanced integrated-system approach with tunable piezoelectric circuitry is used, no obvious improvement is observed in the case of *ad hoc* inductance tuning ($\tilde{L}_i = (100 + 10 \times i)$ H; $i = 1, 2, \cdots, 10$), while a quite accurate prediction is achieved when using the *favorable* inductance tuning. This clearly demonstrates the necessity of employing the proposed tuning methodology.

In order to quantitatively evaluate the performance of damage identification using different methods, we define a performance metric as the root-mean-square difference (RMSD) between the predicted stiffness parameter reduction using one specific method ($\delta\boldsymbol{\alpha}^p$) and the actual damage-induced stiffness parameter reduction ($\delta\boldsymbol{\alpha}^a$),

$$\mathrm{RMSD}(\%) = \sqrt{\frac{(\delta\boldsymbol{\alpha}^p - \delta\boldsymbol{\alpha}^a)^{\mathrm{T}}(\delta\boldsymbol{\alpha}^p - \delta\boldsymbol{\alpha}^a)}{(\delta\boldsymbol{\alpha}^a)^{\mathrm{T}}(\delta\boldsymbol{\alpha}^a)}} \times 100. \tag{40}$$

For the example of damage identification shown in Fig. 12, the prediction obtained from the traditional method results in a RMSD error of 92%, and the predictions obtained from the enhanced integrated-system approach with *ad hoc* inductance tuning and *favorable* inductance tuning have RMSD errors of 73% and 2%, respectively.

In a second example, we detect multiple element damages and the result is shown in Fig. 13, where the actual structural damages are assumed to be on the 2nd and 5th elements with 25% and 15% damage-induced stiffness reductions, respectively. Neither the traditional method nor the enhanced integrated-system approach with *ad hoc* inductance tuning gives an accurate prediction of the actual damage situation. When the enhanced integrated-system approach with the *favorable* inductance tuning is used, both the locations and severities of the two damages are accurately predicted. In terms of the RMSD error of the different methods, the prediction obtained from the traditional method results in a RMSD error of 60%, and the predictions obtained from the enhanced integrated-system approach with *ad hoc* inductance tuning and *favorable* inductance tuning have RMSD errors of 45% and 5%, respectively.

Since measurement noise is inevitable in practical applications, it is necessary to investigate the effects of measurement noise on the damage identification performance of the proposed approach. The effects of measurement noise on the measured eigenvalues (natural frequencies) can be simulated using the following equation:

$$\tilde{\boldsymbol{\lambda}}^d = \boldsymbol{\lambda}^d + v\mathbf{R}\boldsymbol{\lambda}^d, \tag{41}$$

where $\tilde{\boldsymbol{\lambda}}^d$ is the noise-contaminated eigenvalues, $\boldsymbol{\lambda}^d$ is the noise-free eigenvalue, $\mathbf{R}$ is a diagonal matrix whose diagonal entries are independently, uniformly distributed random numbers in the interval of $[-1, 1]$, and v represents the noise level. The noise-contaminated eigenvalue measurement with two different noise levels, $v = 1.0\%$ and 2.0%, are used to identify the same damage scenario as given in Fig. 13, and the damage identification results are shown in Fig. 14. Compared with the result using noise-free eigenvalue measurement, the inclusion of measurement noise in the measured eigenvalues only leads to small variations in the damage identification results. In other words, the overall damage characteristics (locations and severities) are still successfully identified.

5.2. Damage identification in the cantilevered plate with tunable piezoelectric circuitry network

In this second case study, we will examine the performance improvement of using multiple tunable piezoelectric circuitries to detect damages in a more complicated plate structure, and we also compare the damage detection performance by using different tuning options. In this example, we assume that only the

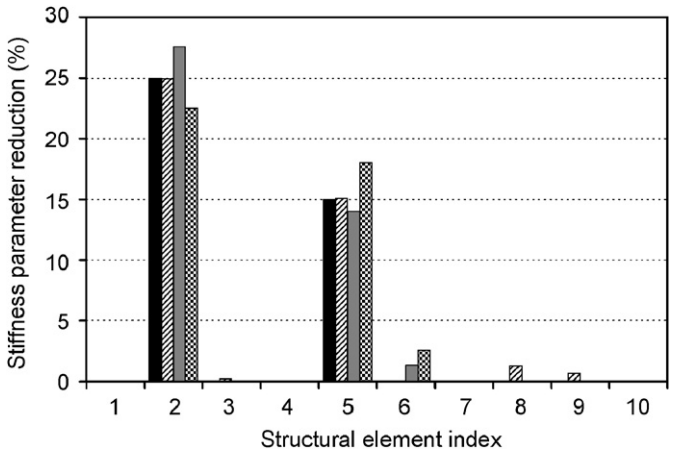

Fig. 14. Comparison of damage identification results using noise-free and noise-contaminated eigenvalues of the integrated beam system. The damages are assumed to cause 25% and 15% stiffness reduction on the second and fifth elements, respectively. ■ Actual stiffness parameter reduction, ▨ prediction using noise-free eigenvalues, ▩ prediction using noise-contaminated eigenvalues ($v = 1.0\%$), ▩ prediction using noise-contaminated eigenvalues ($v = 2.0\%$).

frequencies under 4000 rad/s are available for accurate measurement. Therefore, only the first five natural frequencies can be used for damage identification when we use the traditional method without tunable piezoelectric circuitry, and only the first eight natural frequencies, of which the additional three come from the inductance circuit connected to the piezoelectric transducer, are available when using the enhanced method with integration of tunable piezoelectric circuitry. According to the two tuning options derived in the previous section, the first set of inductance tuning sequence can be selected from the inductance tuning ranges obtained for tuning option 1,

$$\begin{Bmatrix} \mathbf{L}^{(1)} \\ \mathbf{L}^{(2)} \\ \mathbf{L}^{(3)} \\ \mathbf{L}^{(4)} \\ \mathbf{L}^{(5)} \end{Bmatrix} = \begin{bmatrix} L_1^{(1)} & L_2^{(1)} & L_3^{(1)} \\ L_1^{(2)} & L_2^{(2)} & L_3^{(2)} \\ L_1^{(3)} & L_2^{(3)} & L_3^{(3)} \\ L_1^{(4)} & L_2^{(4)} & L_3^{(4)} \\ L_1^{(5)} & L_2^{(5)} & L_3^{(5)} \end{bmatrix} = \begin{bmatrix} 78.6 & 1.51 & 14.00 \\ 81.6 & 1.61 & 14.15 \\ 84.6 & 1.71 & 14.30 \\ 87.6 & 1.81 & 14.45 \\ 90.6 & 1.91 & 14.60 \end{bmatrix} \text{H.} \tag{42}$$

A second set of inductance tuning sequence is selected from the inductance tuning ranges obtained for tuning option 2

$$\begin{Bmatrix} \mathbf{L}^{(1)} \\ \mathbf{L}^{(2)} \\ \mathbf{L}^{(3)} \\ \mathbf{L}^{(4)} \\ \mathbf{L}^{(5)} \end{Bmatrix} = \begin{bmatrix} L_1^{(1)} & L_2^{(1)} & L_3^{(1)} \\ L_1^{(2)} & L_2^{(2)} & L_3^{(2)} \\ L_1^{(3)} & L_2^{(3)} & L_3^{(3)} \\ L_1^{(4)} & L_2^{(4)} & L_3^{(4)} \\ L_1^{(5)} & L_2^{(5)} & L_3^{(5)} \end{bmatrix} = \begin{bmatrix} 0.51 & 0.65 & 1.16 \\ 0.71 & 0.95 & 1.56 \\ 0.91 & 1.25 & 1.96 \\ 1.16 & 1.55 & 2.36 \\ 1.41 & 1.85 & 2.66 \end{bmatrix} \text{H.} \tag{43}$$

As showing in Figs. 8 and 10, respectively, each set of the inductance tuning sequence formulated above achieves one set of eigenvalue curve veering between different pairs of system eigenvalues, and the ability of accomplishing multiple sets of eigenvalue curve veering is exactly the additional benefit offered by integrating multiple piezoelectric circuitries. Therefore, to utilizing multiple sets of eigenvalue curve veering to further enrich the frequency measurement data for damage detection, the inductances should be tuned according to a combined inductance tuning sequence, which can be obtained by assembling the two sets of inductance tuning sequences in Eqs. (42) and (43),

$$\begin{bmatrix} L_1^{(1)} & L_1^{(2)} & \cdots & L_1^{(10)} \\ L_2^{(1)} & L_2^{(2)} & \cdots & L_2^{(10)} \\ L_3^{(1)} & L_3^{(2)} & \cdots & L_3^{(10)} \end{bmatrix} = \begin{bmatrix} 78.6 & 81.6 & 84.6 & 87.6 & 90.6 & 0.51 & 0.71 & 0.91 & 1.16 & 1.41 \\ 1.51 & 1.61 & 1.71 & 1.81 & 1.91 & 0.65 & 0.95 & 1.25 & 1.55 & 1.85 \\ 14.00 & 14.15 & 14.30 & 14.45 & 14.60 & 1.16 & 1.56 & 1.96 & 2.36 & 2.66 \end{bmatrix} \text{H.} \tag{44}$$

Table 3
Natural frequencies of the integrated plate system with respect to inductance tuning

Inductance (H)			System natural frequencies (rad/s)							
L_1	L_2	L_3	ω_1	ω_2	ω_3	ω_4	ω_5	ω_6	ω_7	ω_8
78.6	1.51	14.00	281.46	299.38	698.57	704.98	1900.0	2132.4	2385.8	2700.2
81.6	1.61	14.15	280.70	294.64	697.85	702.14	1898.9	2070.5	2381.2	2700.2
84.6	1.71	14.30	279.34	290.76	694.98	701.43	1896.6	2014.0	2378.4	2700.0
87.6	1.81	14.45	277.11	288.05	692.10	700.71	1891.0	1964.7	2376.8	2700.0
90.6	1.91	14.60	273.99	286.44	688.48	700.71	1874.8	1930.3	2375.3	2700.0
0.51	0.65	1.16	283.23	699.86	1901.6	2331.1	2471.8	2700.9	3279.3	3689.9
0.71	0.95	1.56	283.23	699.86	1900.0	2101.9	2358.0	2698.3	2725.6	3130.8
0.91	1.25	1.96	283.23	699.86	1866.8	1912.1	2295.4	2434.7	2695.7	2771.6
1.16	1.55	2.36	283.23	699.86	1710.6	1901.1	2107.1	2373.0	2460.3	2701.5
1.41	1.85	2.66	283.23	699.86	1612.5	1887.1	1948.6	2215.6	2383.3	2700.7

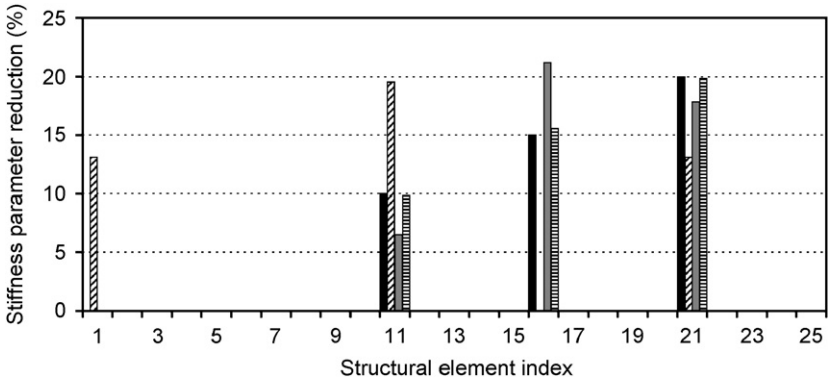

Fig. 15. Identification of damages on the 11th, 16th and 21st elements of the plate structure with 10%, 15% and 20% stiffness parameter reductions, respectively. ■ Actual stiffness parameter reduction, ▨ prediction using the traditional method, ▩ prediction using the enhanced integrated-system approach with *ad hoc* inductance tuning, ▤ prediction using the enhanced integrated-system approach with *favorable* inductance tuning.

Table 4
Damage-induced natural frequency changes of the integrated plate system with respect to inductance tuning

Inductance (H)			Damage-induced natural frequency changes (rad/s)							
L_1	L_2	L_3	$\delta\omega_1$	$\delta\omega_2$	$\delta\omega_3$	$\delta\omega_4$	$\delta\omega_5$	$\delta\omega_6$	$\delta\omega_7$	$\delta\omega_8$
78.6	1.51	14.00	−7.62	−0.67	−8.64	−0.71	−23.57	−0.94	−7.56	−24.55
81.6	1.61	14.15	−7.18	−1.12	−7.93	−1.43	−23.58	−0.97	−7.78	−24.55
84.6	1.71	14.30	−6.34	−1.95	−5.05	−4.29	−23.08	−1.49	−7.79	−24.37
87.6	1.81	14.45	−4.97	−3.35	−2.89	−6.45	−21.00	−3.06	−8.22	−24.37
90.6	1.91	14.60	−3.29	−5.00	−0.73	−8.62	−14.46	−9.87	−8.01	−24.56
0.51	0.65	1.16	−8.28	−9.28	−24.08	−6.66	−1.62	−24.55	−0.15	−0.27
0.71	0.95	1.56	−8.28	−9.28	−23.83	−0.48	−7.65	−23.82	−1.28	−0.32
0.91	1.25	1.96	−8.28	−9.28	−8.86	−14.96	−4.36	−4.11	−23.85	−1.08
1.16	1.55	2.36	−8.28	−9.28	−0.29	−23.29	−0.95	−6.75	−1.22	−24.36
1.41	1.85	2.66	−8.28	−9.27	−0.31	−19.17	−5.14	−0.68	−7.78	−24.55

The damages are assumed to cause 10%, 15% and 20% stiffness reductions on the 11th, 16th and 21st elements, respectively.

Unless otherwise specified, hereafter this combined inductance tuning sequence is used as the favorable tuning sequence in the proposed new method for damage identification.

The variation of the first eight natural frequencies with respect to inductance tuning sequence in Eq. (44) is shown in Table 3. In the first 5 rows in this table, the first 6 natural frequencies vary significantly with respect to inductance tuning. This is because the corresponding inductance tuning sequence is selected from tuning option 1 where eigenvalue curve veering occur between the 1st and 2nd, the 3rd and 4th, and the 5th and 6th system eigenvalues. In the last 5 rows, the 3rd through the 8th natural frequencies vary significantly with respect to inductance tuning because the inductance tuning sequence is selected from tuning option 2 where eigenvalue curve veering occur between the 3rd through the 8th system eigenvalues.

The first example of damage detection is shown in Fig. 15. The actual structural damages, denoted by the solid black bars in this figure, are assumed to be on the 11th, 16th, and 21st elements with 10%, 15%, and 20% stiffness reductions, respectively. The variation of damage-induced frequency shift with respect to inductance tuning sequence is shown in Table 4. Compared to only one set of frequency-shifts when using the traditional method without tunable piezoelectric circuitry, we can now obtain as many sets of frequency-shift measurement as the number of tuned inductance sequence. As shown in Fig. 15, the prediction by using the traditional method has significant RMSD error of 86%, which is not acceptable. Although the enhanced

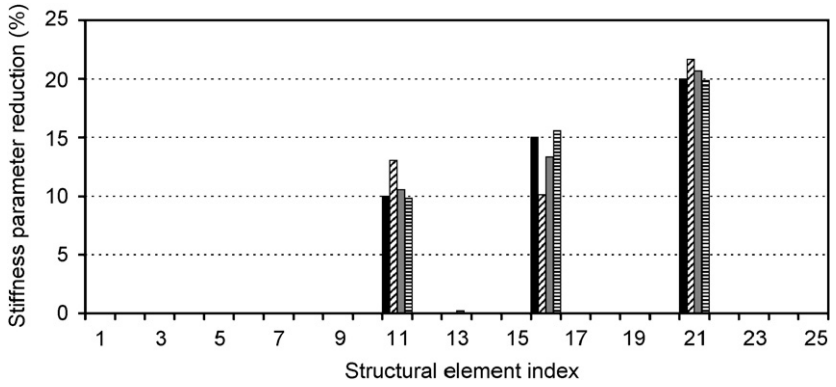

Fig. 16. Effects of different inductance tuning sequences on the performance of damage identification for the plate structure. ■ Actual stiffness parameter reduction, ▨ prediction using tuning option 1, ▩ prediction using tuning option 2, ▤ prediction using the combined tuning option.

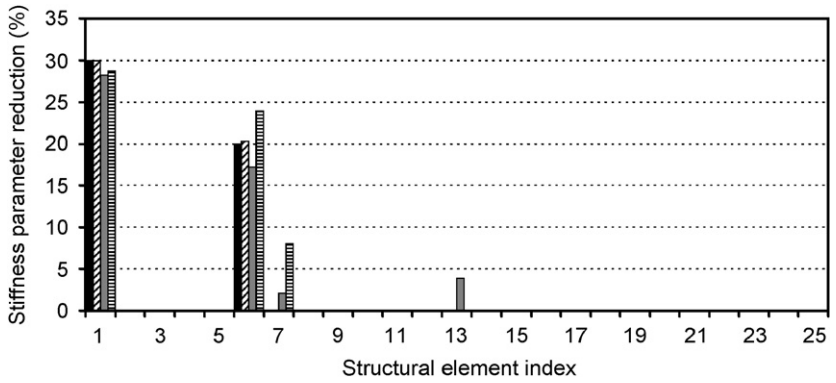

Fig. 17. Comparison of damage identification results using noise-free and noise-contaminated eigenvalues of the integrated plate system. The damages are assumed to cause 30% and 20% stiffness reduction on the first and sixth elements, respectively. ■ Actual stiffness parameter reduction, ▨ prediction using noise-free eigenvalues, ▩ prediction using noise-contaminated eigenvalues ($v = 0.5\%$), ▤ prediction using noise-contaminated eigenvalues ($v = 1.0\%$).

integrated-system approach with *ad hoc* inductance tuning ($\tilde{L}_1^{(i)} = (i)\,\mathrm{H}$, $\tilde{L}_2^{(i)} = (2 \times i - 1)\,\mathrm{H}$, $\tilde{L}_3^{(i)} = (3 \times i - 2)\,\mathrm{H}$, where $i = 1, 2, \cdots, 10$) successfully locate all three damaged elements, the predicted damage severities are not accurate and have a RMSD error of 28%. When the enhanced integrated-system approach with *favorable* inductance tuning is used, the three locations of the structural damages are exactly identified, and the predicted damage severities are very close to the actual stiffness parameter reductions. The RMSD error of the prediction by using the *favorable* inductance tuning is only 2%.

In order to further examine the effects of inductance tuning sequence on the performance of damage detection, the predictions using three different sets of inductance tuning sequences are compared in Fig. 16. The first set of inductance tuning sequence is selected from tuning option 1, as shown in Eq. (42), the second set of tuning sequence is selected from tuning option 2, as shown in Eq. (43), and the third set is the combination of the first two sets, as given by Eq. (44). As shown in the Fig. 16, the locations of the three damaged elements are accurately predicted by using any set of the inductance tuning sequence. However, the predicted severities of the three damages have a RMSD error of 22% when using the tuning option 1. When tuning option 2 is used, the predicted severities are much more accurate and the prediction error in terms of RMSD decreases to 7%. The performance improvement is not only because the eigenvalue curve veering is achieved for high-order system eigenvalues which are usually more sensitive to structural damage than low

eigenvalues, but also because of the more noticeable variation of damage-induced eigenvalue change with respect to inductance tuning as shown in Fig. 11. Finally, when the combined tuning sequence is used, the accuracy of the predicted damage severities is further improved with a prediction error of 2%.

The above case study clearly demonstrates the merits of using multiple piezoelectric transducer circuitries to detect damage. To best benefit the damage identification process, the *favorable* inductance tuning sequence for the tunable piezoelectric circuitry network can be formed by accomplishing a "comprehensive" set of eigenvalue curve veering in the sense that each of the measurable modal frequencies is under curve veering at least once.

Another case study is performed to illustrate the effects of measurement noise on the performance of damage identification. As shown in Fig. 17, the noise-free and noise contaminated eigenvalues with noise levels of $v = 0.5\%$ and 1.0%, are used to identify 30% stiffness reduction in the 1st element and 20% stiffness reduction in the 6th element. The prediction of damages using noise-free eigenvalues matches very well with the actual damage scenario. When the noise-contaminated eigenvalues are used to perform damage identification, the two damages are also successfully located and the damage severities are also well predicted. Therefore, even in the presence of measurement noise, the proposed damage identification method can still provide a satisfactory prediction of the damage scenario.

6. Conclusion

In this paper, the state-of-the-art of frequency-shift based damage identification method using tunable piezoelectric transducer circuitry is advanced. Particularly, the inductance tuning criterion that can fully take advantage of the frequency measurement enrichment feature of the circuitry is established. Our analysis shows that rapid changes of system eigenvalues with respect to inductance variation occur when eigenvalue curve veering is achieved. Moreover, in the region of eigenvalue curve veering, high sensitivity of damaged-induced eigenvalue changes with respect to inductance tuning can be expected. By tuning the inductance around the curve-veering region, one may obtain a *family* of frequency response functions that could reflect the damage occurrence effectively. When multiple tunable piezoelectric transducer circuitries are integrated to the mechanical structure, multiple eigenvalue curve veering can be simultaneously accomplished, and a series of inductance tunings can be formed by accomplishing curve veering between different pairs of system eigenvalues To best characterize the damage occurrence, the favorable inductance tuning sequence should be selected as that leads to a "comprehensive" set of eigenvalue curve veering, i.e., all measurable resonant frequencies undergo curve veering at least once. A series of case studies are performed to demonstrate the tuning criterion and verify the performance improvement in damage identification practices.

Acknowledgments

This research is supported by the National Science Foundation under the Grant numbers CMS 05-29029 and CMS 05-28790.

References

[1] H. Sohn, C.R. Farrar, F.M. Hemez, D.D. Shunk, D.W. Stinemates, B.R. Nadler, A review of structural health monitoring literature: 1996–2001, Los Alamos National Laboratory Report LA-13976-MS, 2003.

[2] S.W. Doebling, C.R. Farrar, M.B. Prime, A summary review of vibration-based damage identification methods, *Shock and Vibration Digest* 30 (2) (1998) 91–105.

[3] S.W. Doebling, C.R. Farrar, M.B. Prime, D.W. Shevitz, Damage identification and health monitoring of structural and mechanical systems from changes in their vibration characteristics: a literature review, Los Alamos National Laboratory Report LA-13070-MS, 1996.

[4] P. Cornwell, M. Kan, B. Carlson, L.B. Hoerst, S.W. Doebling, C.R. Farrar, Comparative study of vibartion-based damage identification algorithms, *Proceedings of the 16th International Modal Analysis Conference*, Part 2, Santa Barbara, CA, 1998, pp. 1710–1716.

[5] E. Dascotte, Practical application of finite element tuning using experimental modal data, *Proceedings of the 8th International Modal Analysis Conference*, Kissimmee, FL, 1990, pp. 1032–1037.

[6] M.I. Friswell, J.E.T. Penny, The practical limits of damage detection and location using vibration data, *Proceedings of the 11th VPI&SU Symposium on Structural Dynamics and Control,* Blacksburg, VA, 1997, pp. 31–40.
[7] O.S. Salawu, Detection of structural damage through changes in frequency: a review, *Engineering Structures* 19 (9) (1997) 718–723.
[8] L.R. Ray, L. Tian, Damage detection in smart structures through sensitivity enhancing feedback control, *Journal of Sound and Vibration* 227 (5) (1999) 987–1002.
[9] L.R. Ray, B.H. Koh, L. Tian, Damage detection and vibration control in smart plates: towards multifunctional smart structures, *Journal of Intelligent Material Systems and Structures* 11 (9) (2000) 725–739.
[10] B.H. Koh, L.R. Ray, Feedback controller design for sensitivity-based damage localization, *Journal of Sound and Vibration* 273 (1-2) (2004) 317–335.
[11] P.D. Cha, W. Gu, Model updating using an incomplete set of experimental modes, *Journal of Sound and Vibration* 233 (4) (2000) 587–600.
[12] N.G. Nalitolela, J.E.T. Penny, M.I. Friswell, Mass or stiffness addition technique for structural parameter updating, *Modal Analysis: The International Journal of Analytical and Experimental Modal Analysis* 7 (3) (1992) 157–168.
[13] J.-S. Lew, J.N. Juang, Structural damage detection using virtual passive controllers, *Journal of Guidance, Control, and Dynamics* 25 (3) (2002) 419–424.
[14] L.J. Jiang, J. Tang, K.W. Wang, An enhanced frequency-shift based damage identification method using tunable piezoelectric transducer circuitry, *Smart Materials and Structures* 15 (3) (2006) 799–808.
[15] R. Senani, New tunable synthetic floating inductors, *Electronics Letters* 16 (10) (1980) 382–383.
[16] R. Senani, Generation of new two-amplifier synthetic floating inductors, *Electronics Letters* 23 (22) (1987) 1202–1203.
[17] M.T. Abuelma'atti, M.H. Khan, Current-controlled OTA-based single-capacitor simulations of grounded inductors, *International Journal of Electronics* 78 (5) (1995) 881–885.
[18] M.O. Cicekoglu, Active simulation of grounded inductors with CCII+s and grounded passive elements, *International Journal of Electronics* 85 (4) (1998) 455–462.
[19] S.J.G. Gift, New simulated inductor using operational conveyors, *International Journal of Electronics* 91 (8) (2004) 477–483.
[20] G.S. Agnes, Development of a modal model for simultaneous active and passive piezoelectric vibration suppression, *Journal of Intelligent Material Systems and Structures* 6 (4) (1995) 482–487.
[21] M.S. Tsai, K.W. Wang, On the structural damping characteristics of active piezoelectric actuators with passive shunt, *Journal of Sound and Vibration* 221 (1) (1999) 1–22.
[22] J. Tang, Y. Liu, K.W. Wang, Semi-active and active-passive hybrid structural damping treatments via piezoelectric materials, *Shock and Vibration Digest* 32 (3) (2000) 189–200.
[23] J. Tang, K.W. Wang, Vibration confinement via optimal eigenvector assignment and piezoelectric network, *Transactions of the ASME: Journal of Vibration and Acoustics* 126 (1) (2004) 27–36.
[24] C.N. Wong, W.D. Zhu, G.Y. Xu, On an iterative general-order perturbation method for multiple structural damage detection, *Journal of Sound and Vibration* 273 (1-2) (2004) 363–386.
[25] A.W. Leissa, On a curve veering aberration, *Journal of Applied Mathematics and Physics (ZAMP)* 25 (1974) 99–111.
[26] J.R. Kutter, V.G. Sigillito, On curve veering, *Journal of Sound and Vibration* 75 (1981) 585–588.
[27] N.G. Perkins, C.D. Mote Jr., Comments on curve veering in eigenvalue problems, *Journal of Sound and Vibration* 106 (3) (1986) 451–463.
[28] C. Pierre, Mode localization and eigenvalue loci veering phenomena in disordered structures, *Journal of Sound and Vibration* 126 (3) (1988) 485–502.
[29] X.L. Liu, Behavior of derivatives of eigenvalues and eigenvectors in curve veering and mode localization and their relation to close eigenvalues, *Journal of Sound and Vibration* 256 (3) (2002) 551–564.